NONLINEAR EFFECTS IN LONG RANGE PROPAGATION

Kaëlig Castor,[1] Peter Gerstoft, W. A. Kuperman,[1] Gerald L. D'Spain,[1] and B. Edward McDonald[2]

Scripps Institution of Oceanography[1] and Naval Research Laboratory[2]

Sponsored by Defense Threat Reduction Agency

Contract No. DTRA01-00-C-0084

ABSTRACT

The Nonlinear Progressive Wave Equation (NPE) (McDonald and Kuperman, 1987) computer code was coupled with a linear normal mode code in order to study propagation from a high-intensity source in either shallow or deep water. Simulations using the coupled NPE/linear code are used to study both harmonic (high-frequency) and parametric (low-frequency) generation and propagation in shallow or deep water with long-range propagation paths. Included in the modeling are both shock dissipation and linear attenuation. The results of these studies are presented.

OBJECTIVE

Linear acoustic propagation in a waveguide has been studied extensively theoretically, numerically and experimentally. In case of a large underwater explosion, nonlinear processes affect the properties of the acoustic wave. One can expect to characterize and localize nuclear underwater explosions by examining spectrograms, which would show this specific nonlinear behavior (Kuperman et al, 2001; D'Spain et al 2000; Gerstoft, 1999).

The aim of this paper is to highlight the nonlinear phenomena of acoustical propagation such as the nonlinear steepening and shock dissipation. The nonlinear scar in a pulse propagated over long ranges is discussed. Work on this topic has also been carried out by B. Ed McDonald (2002).

Introduction

The nonlinear progressive wave equation (NPE) (McDonald *et al*, 1987; McDonald, 2000, 2002) has been developed to investigate nonlinear acoustic effects (including shocks) in an ocean waveguide. This model assumes propagation within a narrow angle and provides an alternative to the linear parabolic equation (PE) and normal mode (NM) approaches. The model is derived from the Euler equations of fluid dynamics retaining lowest order nonlinearity augmented by an adiabatic equation of state relating pressure and density. The NPE is cast in a wave-following coordinate system moving at a nominal average sound speed c_0 in a preferred propagation direction r. For azimuthally symmetric propagation, the NPE in cylindrical (r, z) coordinates is

$$\frac{\partial R}{\partial t} = -\frac{\partial}{\partial r}\left(c_1 R + \frac{b\, c_0}{2} R^2 \right) - \frac{c_0}{2}\frac{R}{r} - \frac{c_0}{2}\int_{rf}^{r} \frac{\partial^2 R}{\partial z^2} dr \,, \tag{1}$$

where b is the nonlinear parameter (≈3.5 for the ocean), c_1 is the environmental sound speed fluctuation about c_0. $R = r'/r_0$ is the dimension-less density perturbation where r_0 is the unperturbed density and $r' = r - r_0$. The NPE can be also formulated in terms of a dimension-less pressure variable $Q = p'/r_0 c_0^2$ by substituting R with Q in Eq. (1) (Ambrosiano *et al*, 1990). The terms on the right hand side of Eq. (1) represent from left to right, refraction, nonlinear steepening, radial spreading, and diffraction. The quadratic nonlinearity in Eq.(1) implies that the nonlinear contribution to the local sound speed is $b\, c_0 R$. A linear propagation mode can be invoked in the code simply by setting $b = 0$. The water is assumed to be an inviscid fluid and linear attenuation in the sediment layer was included.

RESEARCH ACCOMPLISHED

The nonlinear propagation of an acoustic wave induces-high frequency harmonics. Furthermore, the nonlinear interaction of two monochromatic waves at frequencies f_1 and f_2 propagating in the same direction leads to a secondary radiation at frequencies $f_2 \pm f_1$. This parametric interaction effect is commonly used in many applications such as transducer realization providing high focused underwater acoustic intensity for active sonar; this effect is also used for measurements of the nonlinear parameter in liquids or biologic environments and solids (Barriere, 2002; Marchal, 2002; Lee *et al*, 1995; Hamilton *et al*, 1998).

The work presented in this paper focuses on the physical phenomena that influence the spectral distribution of the energy during propagation in order to understand the characteristics of acoustic signals measured after long-range nonlinear propagation. For this purpose, acoustic propagation for different source waveforms is investigated.

Two narrowband sources in shallow water

All the results presented in this section are for a 200-m depth Pekeris waveguide (Fig. 1.a.). The sound speed in the water column is 1500 m/s and is 1550 m/s in the sediment. At a source depth of 100 m, the NPE code is initialized by a sum of two narrowband sources centered at frequencies f_1=275 Hz and f_2=425 Hz, respectively (Fig. 2.a and 2.d). The wave packet is modulated by two Gaussian envelopes in depth and range. This source allows the study of spectral evolution of the acoustic waves due to nonlinearity within the propagation. High-frequency sources are convenient to get narrow frequency bands and to observe both harmonic and parametric generation. The aim of this section is to evaluate the relative energy associated with both effects. Figures 2.c. and 2.d. represent the depth-averaged spectrum for two narrow band sources at the initial range and at the 280-m range where secondary waves created by both parametric ($f_2 \pm f_1$) and harmonic ($2f_1$ & $2f_2$) effects appear clearly. Higher order radiation with low amplitudes at other different frequency combinations, $2(f_2 - f_1) = 300$ Hz, $3(f_2 - f_1) = 450$ Hz, $4(f_2 - f_1) = 600$ Hz, and $f_1+2(f_2 - f_1)=2f_2+f_1=575$ Hz are also distinguishable.

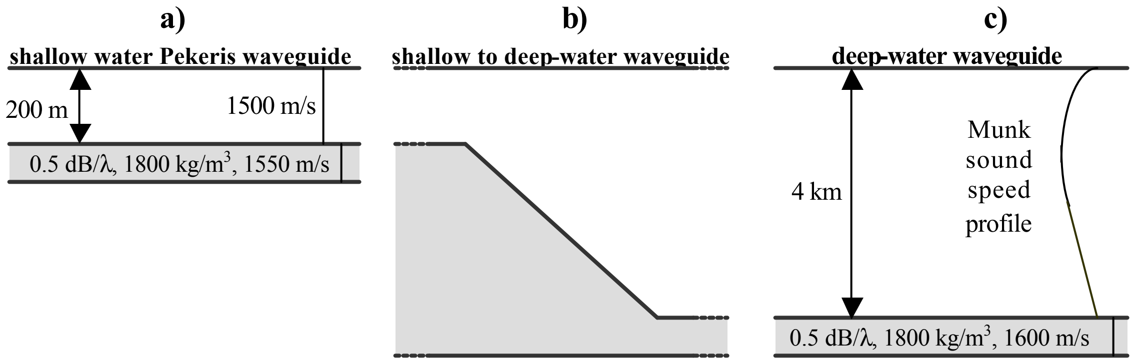

Figure 1. Representation of the environments used in the simulations.

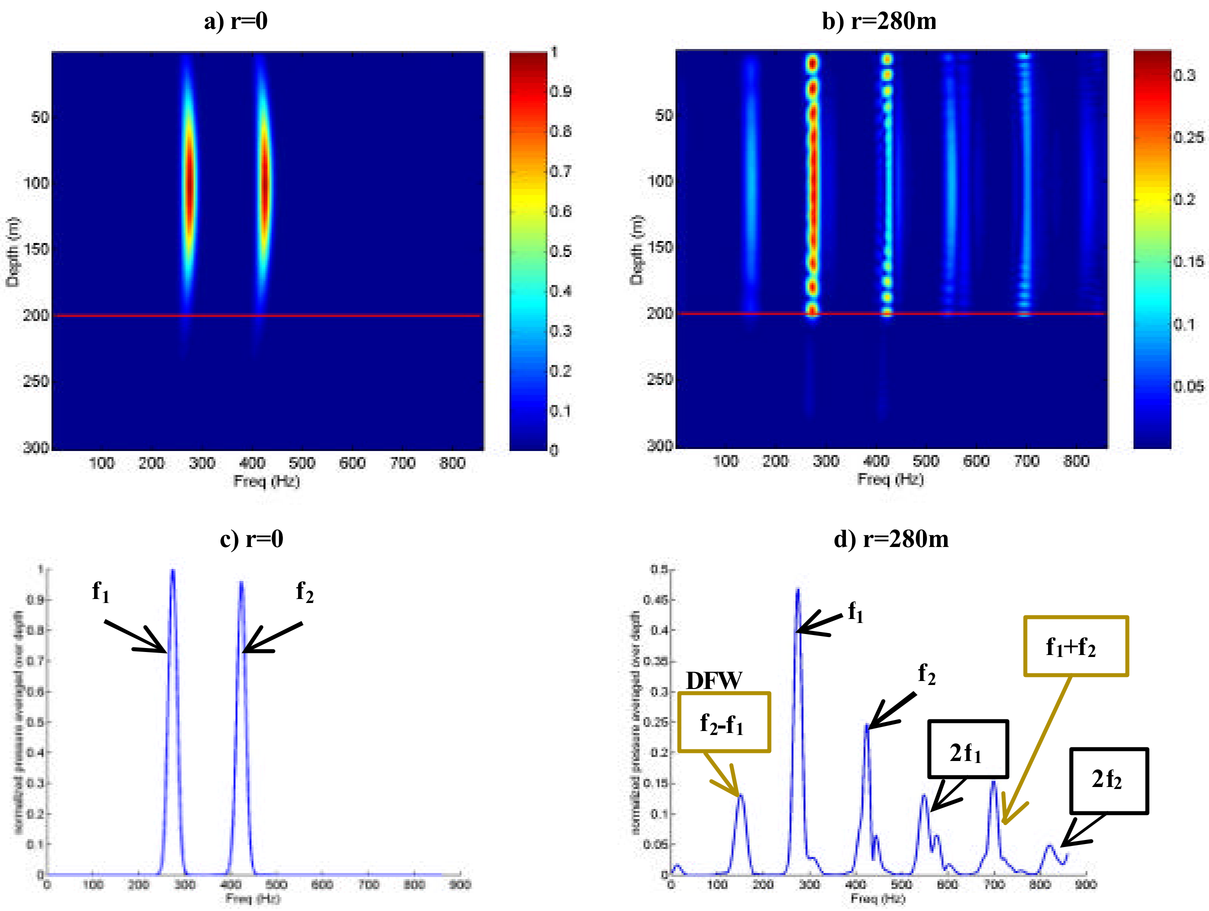

Figure 2: (a & b) Normalized spectrum for two narrow band sources (f_1=275 Hz, f_2=425 Hz) with a source overdensity $R_m=3.10^{-3}$. (c & d) Normalized depth-averaged spectrum. (a & c) range=0. (b & d) range=280m.

Figure 3.a. represents for different maximum overdensity levels R_m the normalized total energy defined by

$$E_T(r) = \sum_i \left|p(f_i, r)\right|^2 \Big/ \sum_i \left|p(f_i, r=0)\right|^2 , \tag{2}$$

where $\left| p(f_i, r) \right|$ is the amplitude of the pressure at the frequency f_i and at the range *r*. Even if the total energy is higher for a high source level, Figure 3(a). shows that the relative losses are much larger for high initial amplitudes since nonlinear effects induce shock dissipation in addition to classical linear absorption.

The only parametric effect considered here is the difference frequency wave (DFW) generation, which is directly related to the low-frequency generation. Figures 3(b) and 3(c) show the energy ratios E_h and E_p, respectively, associated to harmonics and DFW, which are expressed as follows

$$E_h(r) = \left(\left|p(2f_1, r)\right|^2 + \left|p(2f_2, r)\right|^2\right) \Big/ E_i \tag{3}$$

$$\text{and } E_p(r) = \left|p(f_2 - f_1, r)\right|^2 \Big/ E_i , \tag{4}$$

with the initial energy E_i calculated such that

$$E_i = \left|p(f_1, r=0)\right|^2 + \left|p(f_2, r=0)\right|^2 . \tag{5}$$

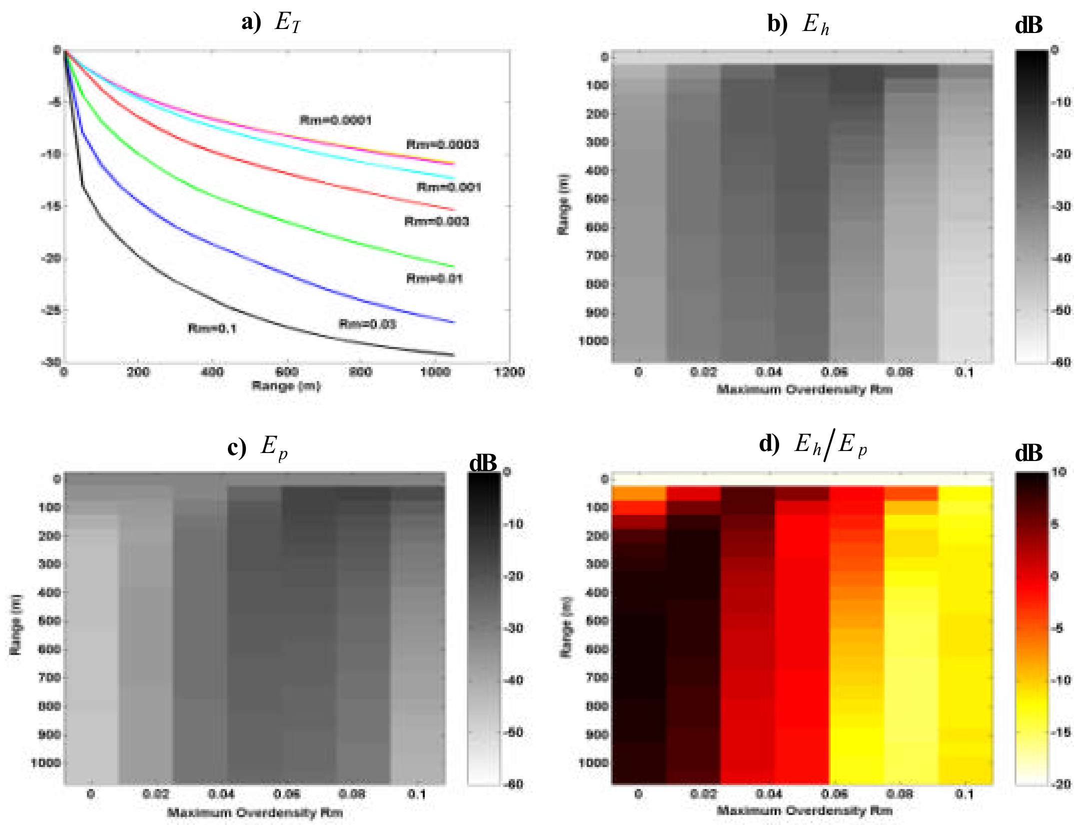

Figure 3: Energy ratios versus range and source overdensity R_m.: (a) Total energy E_T, Eq. (2). (b) Energy in the first harmonic components E_h, Eq. (3). (c) Energy in the parametric difference frequency component E_p, Eq. (4). (d) Energy ratio E_h / E_p.

Near the source, both parametric DFW (E_p) and harmonic (E_h) energy increase for larger source overdensity until an optimum is reached (Fig. 3(b) and 3(c). Both nonlinear effects are in competition with shock wave dissipation. The shock wave leads to an energy absorption process in addition to the intrinsic attenuation. When a discontinuity appears in the waveform profile, the shock wave formation distance is reached. For a shock wave, a cascade of higher frequencies is generated (Hamilton, 1998). This phenomenon increases entropy locally and constitutes a mechanism of energy dissipation even in a perfect fluid. This shock wave formation distance decreases when the source level increases. Thus, for a strong explosion, nonlinearities are important and shock dissipation occurs at shorter ranges and leads to a high-energy decay.

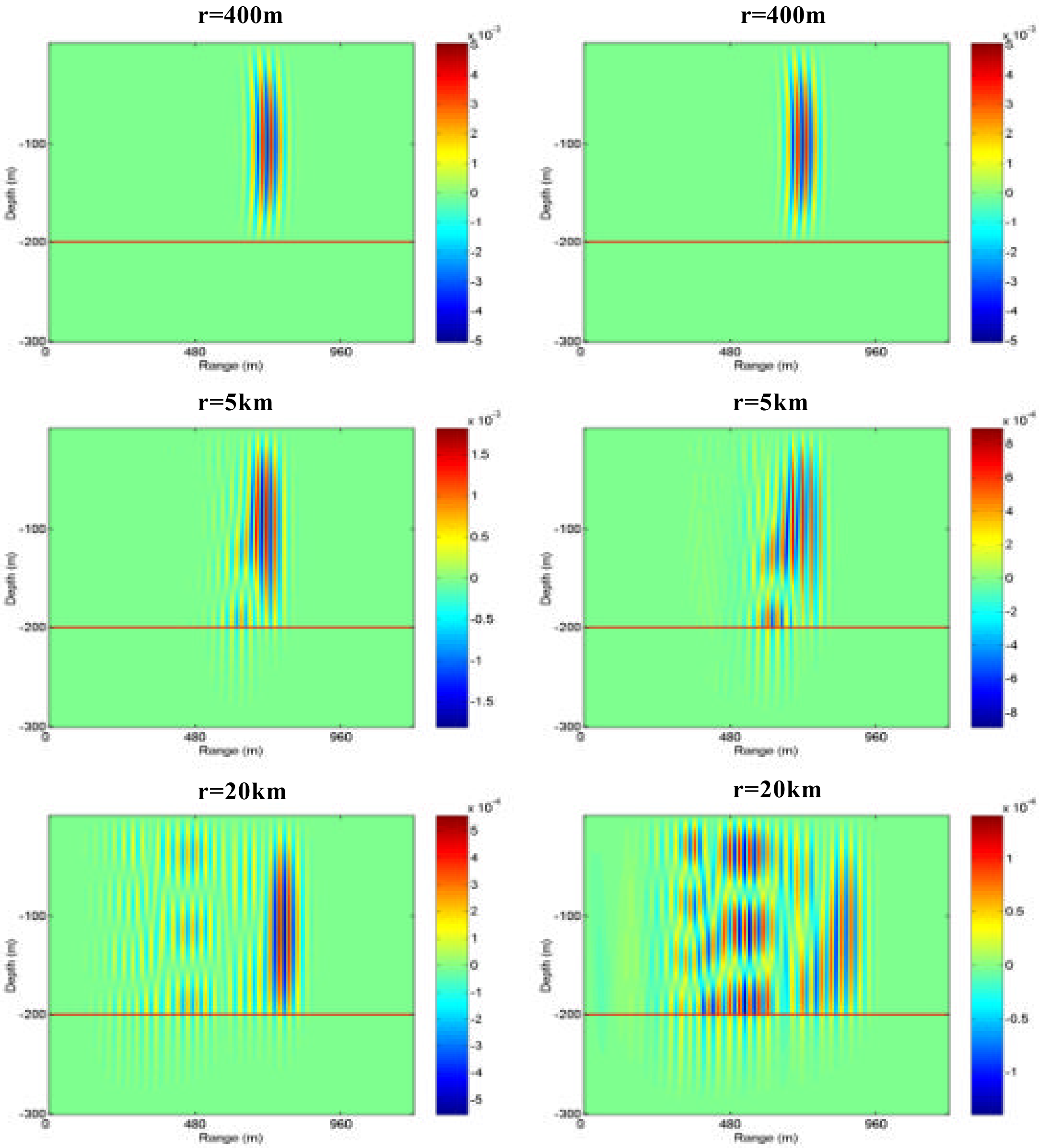

Figure 4: Snapshots at different ranges (400 m, 5 km, 20 km) for both linear (left) and nonlinear (right) shallow water cases with a single narrow band source centered at 50 Hz with a source overdensity R_m= 3.5 10^{-3}.

Finally, even if harmonic (Fig. 3[b]) and difference frequency (Fig. 3[c]) generation have almost the same behavior versus range, there is a weak shift between maximum overdensities for which respective normalized energies E_h and E_p are maximal. Since absorption is more important at higher frequencies, harmonics are damped faster during propagation than the DFW. These observations are also relevant for Figure 3(d), which shows the ratio E_h/E_p . In this figure, three parts can be distinguished: The first part is for low-source overdensities where the shock wave formation distance is large. The harmonic generation due to the nonlinear steepening is greater than the parametric DFW. In the second part, for intermediate levels, both nonlinear effects are of similar importance. In the third part, for high-amplitude source, the shock wave formation distance is shorter. Strong absorption occurs then at short ranges and leads to harmonic dissipation. The low difference frequency wave is thus predominant.

Single narrowband source

In this section, the source conditions are a five-cycle sine-wave packet with a center frequency of 50 Hz, modulated by Gaussian envelopes in depth and range. Figure 4 shows snapshots at different ranges for linear and nonlinear propagation in the Pekeris shallow water waveguide defined in part A (Fig. 1[a]). Corresponding time series are represented in Figure 5 at the source depth (100 m).

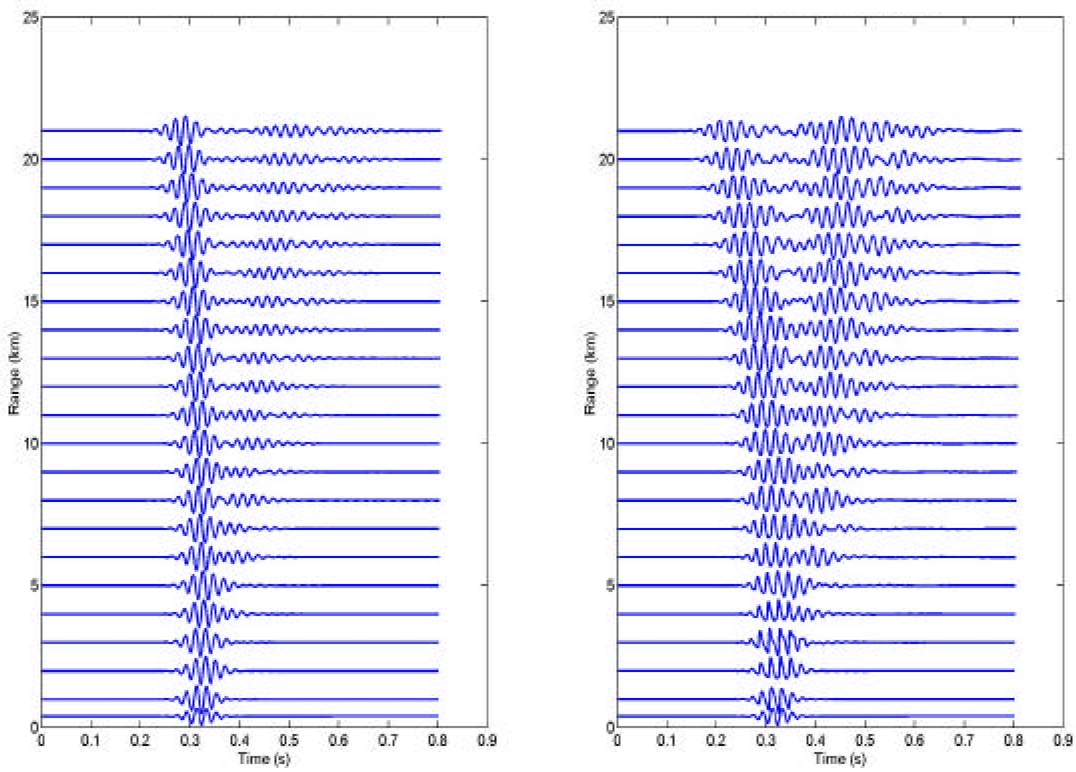

Figure 5: Time series at the source depth (100 m) for linear (left) and nonlinear (right) shallow water cases with a single narrowband source centered at 50 Hz with a source overdensity R_m= 3.5 10^{-3}.

Even though the presence of nonlinearity does not lend itself to straightforward representation in linear normal modes, similarities between the two cases are expected since the nonlinearities are weak. The modal dispersion can be seen in both cases (Fig. 4). At 20-km range, four modes can be distinguished, and one can observe that the lower order modes travel faster. Because nonlinear effects lead to low- and high-frequency generation, the spectral distribution of the energy is generally more complicated and spread over a broad frequency band. Consequently, in the nonlinear case there is an energy transfer toward higher modes and the excitation of each mode is more uniform than in the linear case as can be seen at 20-km range in Figure 4. Furthermore, an important difference is the wave steepening (Fig. 5). In the nonlinear case, the wave form starts out sinusoidal, develops a sawtooth profile (range 3-6 km), and ultimately falls victim to effects of dissipation and reverts to a waveform resembling the signal at the source, although much reduced in amplitude (this attenuation is not visible in the time series representation shown in Fig. 5 since all the signals are normalized by their maximum at each range for lisibility). After an initial phase in which the nonlinear wave loses energy to shock processes and increased bottom penetration, its interaction with the waveguide becomes essentially linear. Then, a linear adiabatic normal mode code can be used to propagate the field to much longer ranges (i.e. several hundred kilometers), using less CPU time.

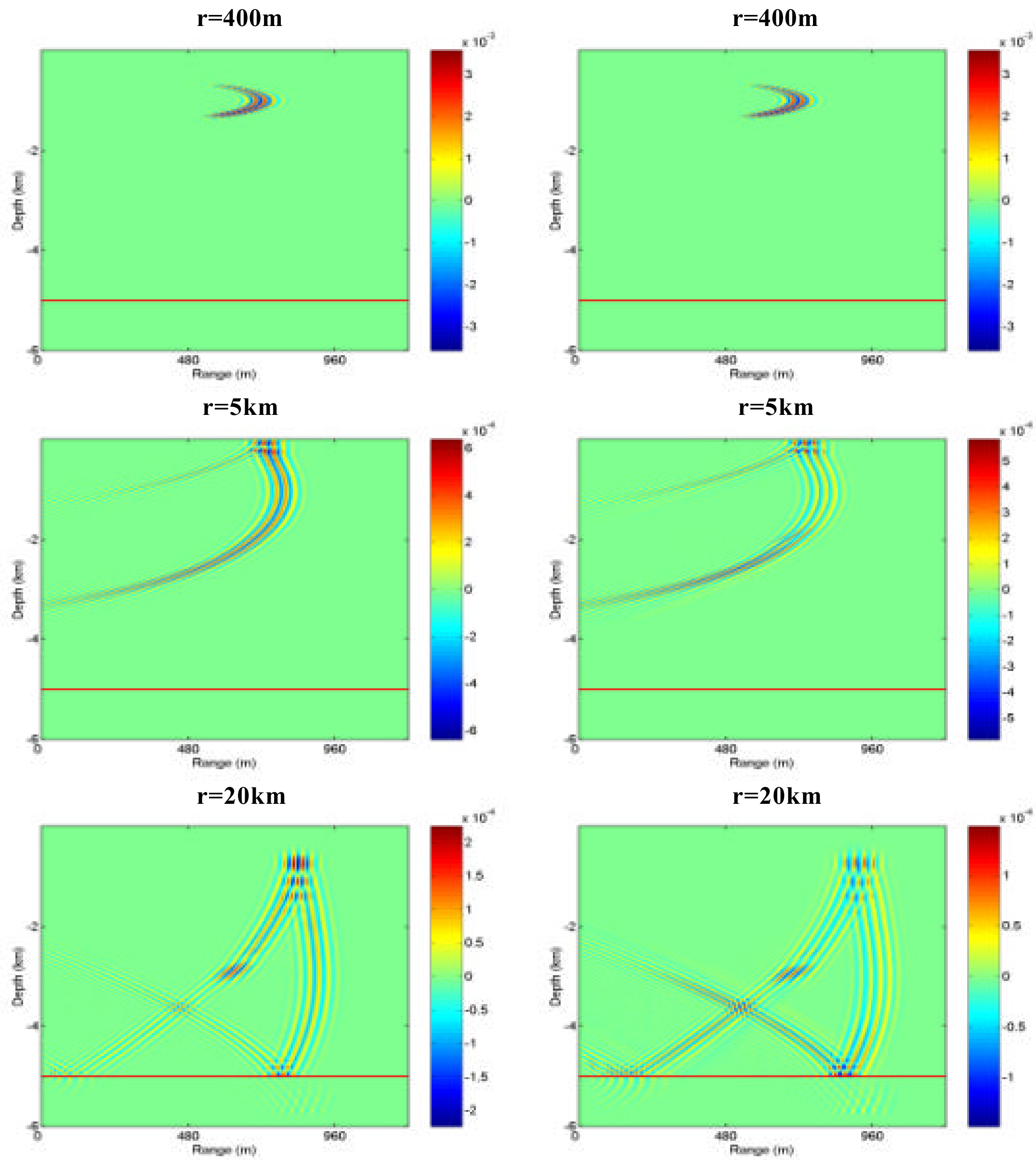

Figure 6: Snapshots at different ranges (400 m, 5 km, 20 km) for both linear (left) and nonlinear (right) deep water cases with a single narrow band source centered at 50 Hz with a source overdensity R_m=3.5 10^{-3}.

With the same source, Figures 6 and 7 show respectively snapshots and time series, at 1 km corresponding to the source depth, for linear and nonlinear cases within a 5-km deep water waveguide. The sound speed in the sediment layer is 1600 m/s and the absorption coefficient is 0.5 dB/λ (Fig. 1.c.). The results show a weak interaction with the sediments and a localization of the energy at a depth where the sound speed is minimum. In the nonlinear case, there is more energy in the tail of the signal and the pulse duration is longer than in the linear case (Fig. 6). For both cases the signal that appears, at about 4 km and 0.8 s in Figure 7, is due to the bottom bounce, and at about 10 km, this signal melts together with the direct arrival.

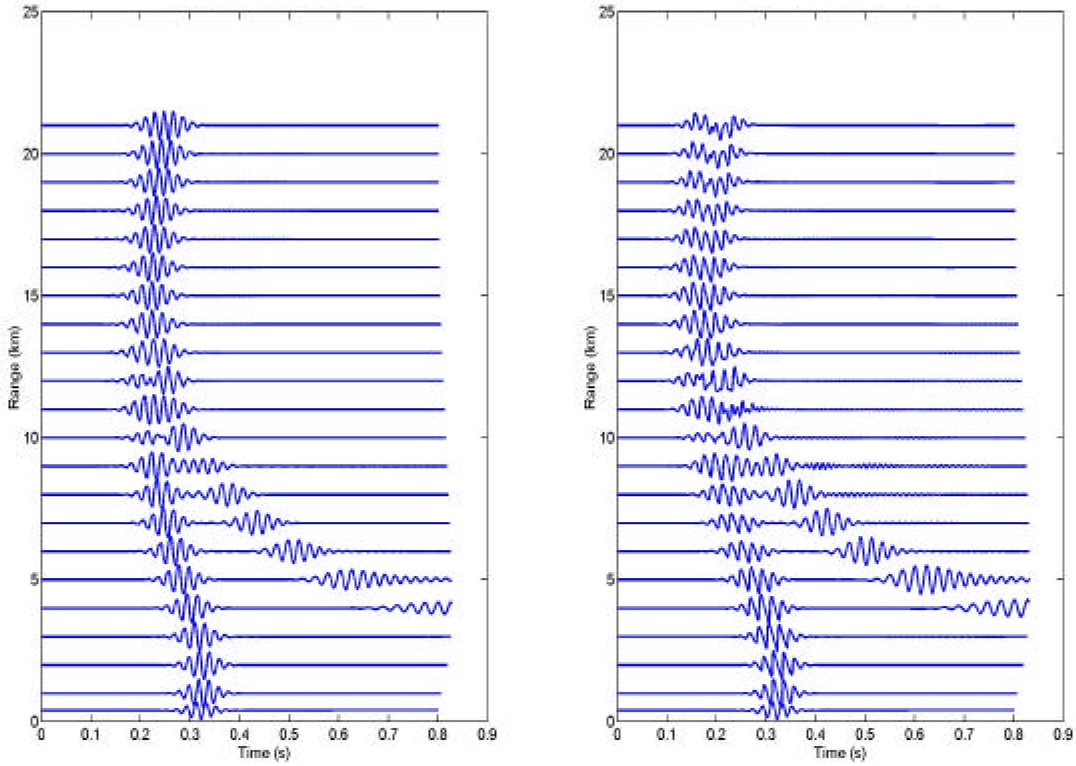

Figure 7: Time series at the source depth (1 km) for linear (left) and nonlinear (right) deep water cases with a single narrowband source centered at 50 Hz with a source overdensity R_m=3.5 10^{-3}.

Figures 8 and 9 compare the influence of the source frequency on the normalized depth averaged spectrum for nonlinear propagation at several ranges. For a 50-Hz source (Fig. 6), one can see both difference-frequency wave Δf (DFW) and harmonic generation. Because of the frequency dependence of the viscous absorption, the waves f, 2f, 3f are damped faster than the DFW. Therefore, only the difference frequency Δf exists at long ranges. There is a tendency for the spectrum to shift toward lower frequencies. However, in the shallow water, Figure 9 shows that the waveguide cut-off frequency (3.75 Hz in this example) limits this tendency for very low frequencies: for a 10-Hz source, the parametric difference frequency wave, related to the source broad frequency band, is not generated since it is below the waveguide cut-off frequency. Also, amplitudes for this 10-Hz source show a weaker dissipation than for the 50-Hz source case.

Below the waveguide cut-off frequency, no mode is generated; thus no modal energy propagates. An important difference between shallow and deep water is this waveguide cut-off frequency, which is greater in shallow water (f_c=3.75 Hz) and leads consequently to eliminate a part of the DFW energy, whereas, in deep water, the waveguide cut-off frequency is much smaller (f_c=0.15 Hz), so DFW generation is less affected in this case.

Long-range propagation

Since the nonlinear effects are important near the source, there is a range for which the amplitude is sufficiently low so that a linear normal mode code can be used to propagate the acoustic field further. The fields from the NPE code at 20 km for both shallow and deep water environments are used as a source in the Kraken normal mode code (Porter, 1991). For the shallow water case, the adiabatic approximation is used to propagate the field to deep water. The snapshots for linear and nonlinear cases are plotted respectively for this shallow-to-deep-water case (Figs. 1[b] and 10) and deep-water case (Fig. 1.c and 11). The results show that the influence of the nonlinear effects on acoustical propagation are greater if the explosion occurs in shallow water. In shallow water, the dispersion of mode-like arrival structures develops more rapidly for a nonlinear case (McDonald, 2002) than when the energy is linearly propagated. When the energy is linearly propagated in deep water, the snapshots keep this different modal dispersion (Fig. 10). The nonlinear effects will cause the frequency spectrum to be broader and will usually excite a broader spectrum of modes, with more relative energy for the high-order modes. This causes a larger time spread. When the signal propagates to deep water, the signals keep this larger time spread (Fig. 10).

In contrast, for deep-water explosions, the nonlinearities do not generate a modal arrival structure, partly because of little interaction with the bottom. The typical modal arrival structure occurs at long ranges where the signals amplitudes are weak and nonlinear effects will not give a larger time spread (Fig. 11).

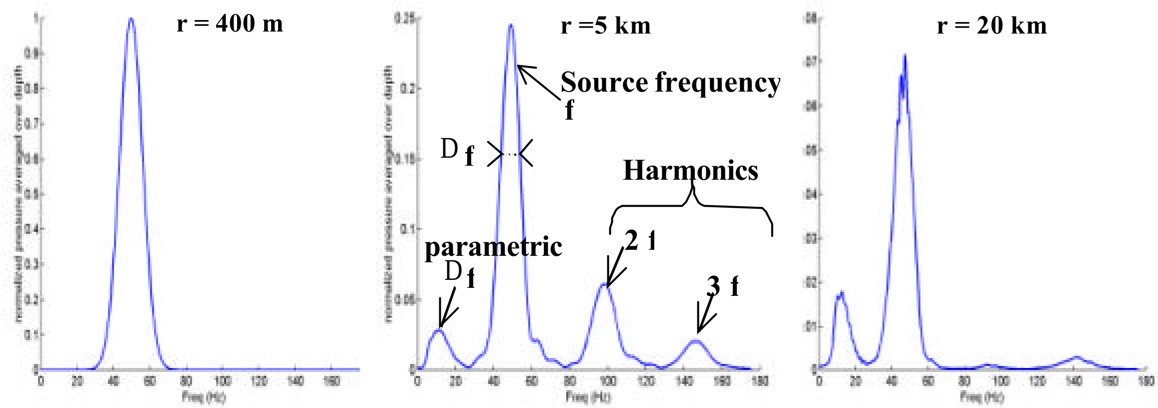

Figure 8: Depth-averaged spectrum at several ranges (r = 400 m, 5 km, and 20 km) for a nonlinear shallow water case with a single narrow frequency band source centered at f = 50 Hz with a source overdensity R_m= 3.5 10^{-3}.

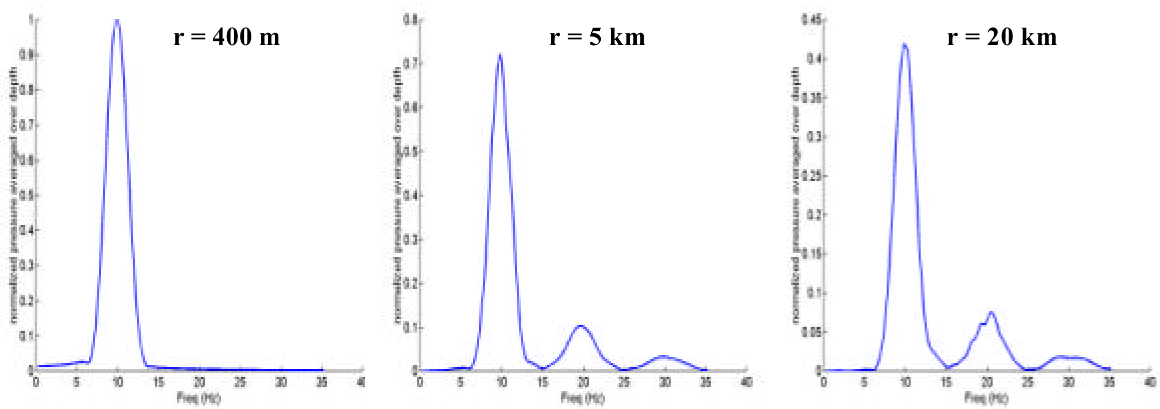

Figure 9: Depth-averaged spectrum at several ranges (r = 400 m, 5 km, and 20 km) for a nonlinear shallow water case with a single narrow frequency band source centered at f = 10 Hz with a source overdensity R_m= 3.5 10^{-3}. Due to the waveguide cut-off frequency, 3.75 Hz, there is no generation of the parametric difference frequencies.

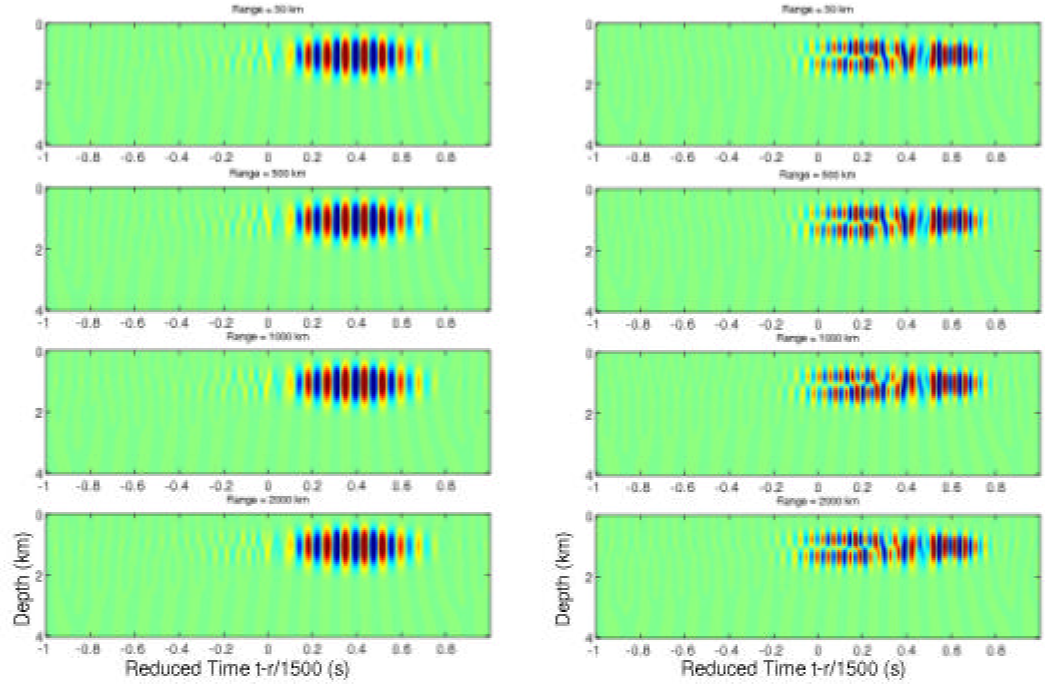

Figure 10: Time series for linear (left) and nonlinear (right) shallow-to-deep-water cases (f = 10 Hz, r = 50 km, 500 km, 1000 km, 2000 km).

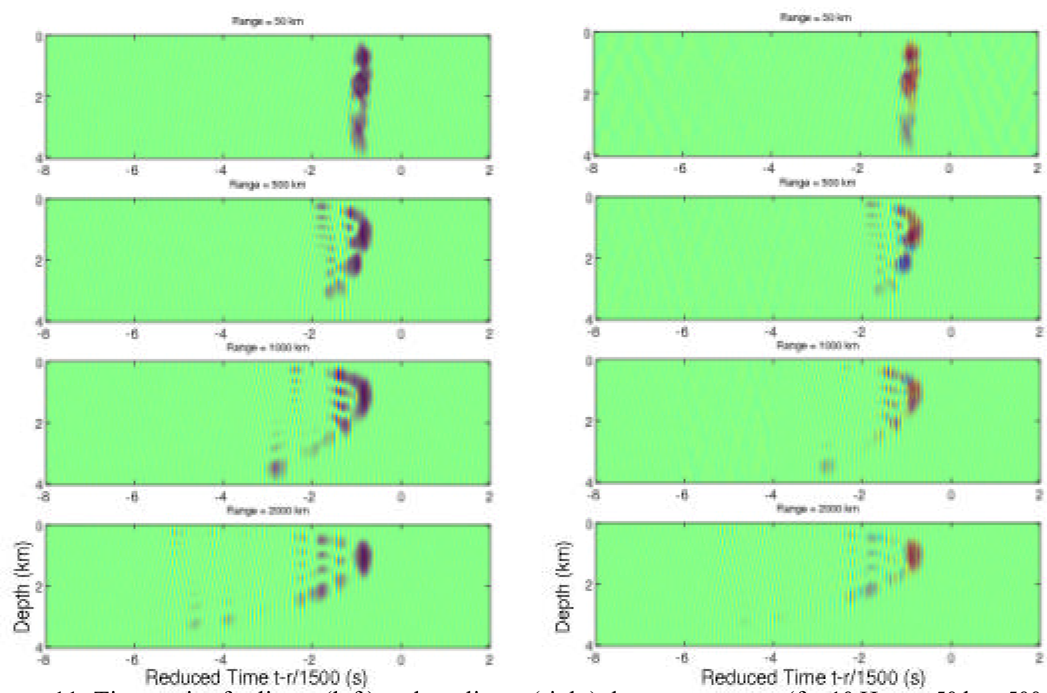

Figure 11: Time series for linear (left) and nonlinear (right) deep water cases (f = 10 Hz, r = 50 km, 500 km, 1000 km, 2000 km).

CONCLUSION AND RECOMMENDATIONS

Results presented here suggest that undersea explosions may be characterized by studying their spectral evolution over long-range nonlinear acoustical propagation. In shallow water, the signal interacts with the bottom earlier than in deep water, thus initially lower geometrical spreading is obtained (cylindrical versus geometric spreading). Therefore, signal amplitudes are initially higher than in the deep water case, causing stronger nonlinear effects. The nonlinear effects will cause the frequency spectrum to be broader and will usually excite a broader spectrum of modes, with more relative energy for the high order modes. In shallow water, low order modes travel faster than high order modes and the nonlinearity will give a larger time spread of the received pulse.

Nonlinear effects on the modal dispersion are much more significant in shallow water than in deep water. Thus, if the event starts in shallow water, it would be easier to discriminate between signals that entered the ocean as linear waves (for example a seismic event or underground explosion) and those that began as nonlinear waves in the ocean itself. In this last case, after long-range propagation, the spectrum is strongly shifted toward low frequencies because of both difference frequency generation and shock dissipation processes. During propagation in shallow waveguide, the lowest frequencies might not be supported by the waveguide, due to modal cut-off. Thus, the low-frequency parametric wave might not always be observed.

ACKNOWLEDGMENTS

The authors are grateful to Philippe Roux for his support and helpful discussions.

REFERENCES

Ambrosiano J. J., D. Plante, B.E. McDonald, W.A. Kuperman (1990), Nonlinear propagation in an ocean acoustic waveguide, *J. Acoust. Soc. Amer.*, **87**, 1473-1481.

Barriere Ch. (2002), Effet de la diffraction sur l'interaction parametrique d'ondes acoustiques. Application a la mesure de parametres de non linearite et de champs acoustiques, PhD dissertation, Universite Denis Diderot-Paris 7.

D' Spain G. L., W.A. Kuperman, J. Orcutt J, and M. Hedlin (2000), Long Range Localization of impulsive sources in the Atmosphere and Ocean from Focus Regions in Single Element Spectrograms, Proc. of 22nd Annual Seismic Research Symposium.

Gerstoft P. (1999), Assessment of hydroacoustic processing in the CTBT release one monitoring software, Comprehensive Nuclear-Test-Ban-Treaty Organisation, Vienna, Austria.

Hamilton M. F. and D.T. Blackstock (1998), *Nonlinear acoustics*, Academic Press.

Kuperman W. A., B.E. McDonald, and G.L. D' Spain (2001), Arrival structure of long-range propagation excited by a finite amplitude source, Proc. of 23rd Annual Seismic Research Symposium.

Marchal J. (2002), Acoustique non lineaire: contribution theorique et experimentale a l'etude de l'emission parametrique, PhD dissertation, Universite Pierre et Marie Curie-Paris 6.

Lee Y. -S. and M.F. Hamilton (1995), Time-domain modeling of pulsed finite-amplitude sound beams, *J. Acoust. Soc. Amer.*, **97**, 906-917.

McDonald B. E. and W.A. Kuperman (1987), Time domain formulation for pulse propagation including nonlinear behavior at a caustic, *J. Acoust. Soc. Amer.*, **81**, 1406-1417.

McDonald B. E. (2000), High-angle formulation for the nonlinear progressive-wave equation model, *Wave Motion*, **31**, 165-171.

McDonald B. E. (2002), Nonlinear effects in source localization, in *Ocean Acoustic Interference Phenomena*, eds. W. A. Kuperman and G. L. D'Spain, AIP Press, NY.

Porter M. (1991), The Kraken normal mode program, SACLANTCEN SM—245.